Revision 1

Supplementary Material

Seismic detectability of carbonates in the deep Earth: a Nuclear Inelastic Scattering study

Stella Chariton[1], Catherine McCammon[1], Denis M. Vasiukov[2], Michal Stekiel[3], Anastasia Kantor[1,4], Valerio Cerantola[4], Ilya Kupenko[5], Timofey Fedotenko[2], Egor Koemets[1], Michael Hanfland[4], Alexandr I. Chumakov[4] and Leonid Dubrovinsky[1]

[1] Bayerisches Geoinstitut, Universität Bayreuth, 95440 Bayreuth, Germany

[2] Laboratory of Crystallography, Universität Bayreuth, 95440 Bayreuth, Germany

[3] Institute of Geosciences, Goethe Universität, 60438 Frankfurt am Main, Germany

[4] ESRF, The European Synchrotron, CS40220, 38043 Grenoble Cedex 9, France

[5] Institute for Mineralogy, Universität Münster, 48149 Münster, Germany

Table S1. Detailed dataset of all Nuclear Inelastic Scattering experiments at room temperature performed in this study.

Sample	Cell #	Type	PTM[a]	P (GPa)	ρ (g/cm^3)	K (GPa)	G (GPa)	Vd (km/s)	Vp (km/s)	Vs (km/s)
$(Mg_{0.74}Fe_{0.26})CO_3$	1	pwdr[b]	-	0.00(0)	3.27 (1)	115.1(5)	61.2(5)	4.82(4)	7.75(2)	4.33(2)
	2	rdm cr[c]	-	0.00(0)	3.27(1)	115.1(5)	55.0(5)	4.58(2)	7.59(2)	4.10(2)
	2	rdm cr	Ar	21.0(3)	3.75(10)	192.9(5)	81.8(5)	5.23(8)	8.97(1)	4.67(1)
	2	rdm cr	Ar	32.6(15)	3.95(18)	231.7(5)	86.9(5)	5.26(7)	9.38(1)	4.69(1)
	2	rdm cr	Ar	40.2(5)	4.07(19)	256.8(5)	93.2(5)	5.37(13)	9.67(1)	4.79(1)
	2	rdm cr	Ar	46.0(15)	4.20(20)	285.6(5)	99.2(5)	5.46(8)	9.97(1)	4.86(1)
	2	rdm cr	Ar	59.0(10)	4.43(20)	353(13)	130(13)	6.10(10)	10.90(22)	5.43(27)
	2	rdm cr	Ar	65.0(10)	4.50(20)	372(13)	134(13)	6.14(14)	11.07(21)	5.47(26)
$FeCO_3$	3	pwdr	Oil[d]	4.4(3)	4.10(5)	137.0(6)	43.9(6)	3.68(2)	6.90(2)	3.27(2)
	3	pwdr	Oil	10.3(3)	4.27(5)	160.0(6)	46.1(6)	3.70(7)	7.20(2)	3.28(2)
	4	rdm cr1	Ar	26.5(5)	4.66(15)	220.0(6)	64.5(7)	4.19(29)	8.10(1)	3.72(2)
	4	rdm cr2	Ar	26.5 (10)	4.66(15)	220.0(6)	68.9(7)	4.33(25)	8.18(1)	3.85(2)
	4	rdm cr1	Ar	40.0 (5)	4.91(19)	263.9(6)	79.0(7)	4.52(24)	8.67(1)	4.01(2)
	4	rdm cr2	Ar	40.0 (15)	4.91(19)	263.9(6)	70.7(6)	4.28(15)	8.54(1)	3.79(2)
	4	pwdr	Ar	54.5(10)	5.73(6)	368(8)	130(8)	5.36(30)	9.72(12)	4.77(15)
	5	pwdr	-	0.00(0)	3.98(6)	121.9(6)	46.8(7)	3.84(5)	6.80(2)	3.43(2)
	6	pwdr	KCl	5.5(5)	4.13(5)	140.9(6)	44.7(6)	3.70(7)	6.96(2)	3.29(2)
	6	pwdr	KCl	22.4(5)	4.58(14)	206.9(6)	62.8(6)	4.17(8)	7.96(1)	3.70(2)

[a] pressure transmitting medium; [b] powdered sample; [c] single-crystal sample with unknown orientation ; [d] paraffin oil

Table S1. (Continued…)

Sample	Cell #	Type	PTM[a]	P (GPa)	ρ (g/cm^3)	K (GPa)	G (GPa)	Vd (km/s)	Vp (km/s)	Vs (km/s)
$FeCO_3$	7	rdm cr[b]	Oil[c]	0.00(0)	3.98(6)	121.9(6)	44.4(7)	3.75(6)	6.74(2)	3.34(3)
	7	rdm cr1	Oil	2.4(5)	4.04(1)	129.3(6)	46.0(6)	3.79(6)	6.87(2)	3.37(2)
	7	rdm cr2	Oil	2.4(5)	4.04(1)	129.3(6)	40.4(6)	3.56(5)	6.73(2)	3.16(2)
	7	rdm cr1	Oil	9.7(5)	4.25(5)	157.2(6)	55.2(6)	4.05(7)	7.37(2)	3.60(2)
	7	rdm cr2	Oil	17.0(5)	4.45(9)	186.5(6)	54.8(6)	3.95(7)	7.63(1)	3.51(2)
	7	rdm cr1	Oil	28.0(5)	4.69(18)	226.8(6)	70.0(6)	4.35(11)	8.25(1)	3.86(2)
	7	rdm cr1	Oil	35.0(5)	4.82(20)	247.6(6)	72.9(7)	4.38(16)	8.46(1)	3.89(2)
	7	rdm cr1	Oil	44.0(5)	5.02(20)	284.6(6)	84.4(7)	4.62(17)	8.89(1)	4.10(2)
	7	rdm cr1	Oil	57.0(5)	5.76(6)	375(8)	139(8)	5.52(18)	9.86(12)	4.91(14)
	7	rdm cr1	Oil	63.0(5)	5.85(7)	395(8)	135(8)	5.40(15)	9.91(11)	4.81(14)
	7	rdm cr1	Oil	65.0(5)	5.88(7)	402(8)	145(8)	5.57(21)	10.05(11)	4.96(14)
	8	pwdr[d]	KCl	37.0(5)	4.86(20)	254.8(6)	81.9(7)	4.62(33)	8.65(1)	4.11(2)
	9	pwdr	KCl	56.0(10)	5.74(6)	370(8)	130(8)	5.35(30)	9.73(12)	4.76(15)

[a] pressure transmitting medium; [b] single-crystal sample with unknown orientation; [c] paraffin oil; [d] powdered sample

Table S2. Comparison of the equations of state parameters of ferromagnesite samples between this study and the literature.

	$FeCO_3$ (This study)		**$(Fe_{0.72}Mg_{0.24}Mn_{0.03}Ca_{0.01})CO_3$**[a] (Lavina et al. 2009,2010a)		**$FeCO_3$**[a] (Zhang et al. 1998)	**$(Fe_{0.60}Mg_{0.38}Mn_{0.02})CO_3$**[a] (Zhang et al. 1998)
Sample type	synthetic crystals		natural crystals		natural powder	natural powder
Method	SCXRD[b]		SCXRD		PXRD[c]	PXRD
Spin state	high	low	high	low	high	high
P range (GPa)[d]	0 – 44.6	46.2 – 66	0 – 43.9	46.4 – 56	0 – 8.9	0 – 8.9
V_0 ($Å^3$)	292.66 (2)[e]	250 (1)[f]	294.4 (3)	263 (3)	292.828 (35)	288.314(133)
K_0 (GPa)	122.0 (6)[g]	172 (8)	110.1(3)	148 (12)	117 (1)	112 (1)
K_0'	4 (fixed)[g]	4 (fixed)	4.6 (2)	5 (fixed)	4 (fixed)	4 (fixed)

	$(Fe_{0.26}Mg_{0.74})CO_3$ (This study)		**$(Fe_{0.12}Mg_{0.87}Ca_{0.01})CO_3$**[a] (Lavina et al. 2010b)		**$(Fe_{0.65}Mg_{0.33}Mn_{0.02})CO_3$**[a] (Lin et al. 2012; Fu et al. 2017)	
Sample type	synthetic crystals		natural crystals		natural powder/crystal	
Method	SCXRD		SCXRD		PXRD	
Spin state	high	low	high	low	high	low
P range (GPa)	0 – 44	48.5 – 59.3	0 – 44.1	48.9 – 64.8	0 – 45	45 – 72
V_0 ($Å^3$)	282.69 (8)[e]	266 (4)[f]	281.0 (5)	-	289.1 (1)	267 (2)
K_0 (GPa)	115.1 (5)[h]	146 (13)	102.8 (3)	-	108 (2)	127 (5)
K_0'	4 (fixed)[h]	4 (fixed)	5.44 (fixed)	-	4.8 (2)	5.1 (2)

	$FeCO_3$ (Stekiel et al. 2017)		**$(Fe_{0.25}Mg_{0.75})CO_3$** (Stekiel et al. 2017)		**$FeCO_3$**[a] (Sanchez-Valle et al. 2014)	**$(Mg_{0.33}Fe_{0.65}Mn_{0.02})CO_3$**[a] (Sanchez-Valle et al. 2014)
Sample type	-		-		natural crystals	natural crystals
Method	DFT[i]		DFT		BLS[j], SCXRD	BLS, SCXRD
Spin state	low	low	high	low	high	high
Pressure (GPa)	0	59	0	59	1 bar	1 bar
$V_{at\ pressure}$ ($Å^3$)	310.12	207.54	287.41	208.64	292.58	290.55
$K_{at\ pressure}$ (GPa)	130.80	393.63	112.48	366.71	116 (2)	113 (2)

[a]see reference for more details on sample's chemical composition; [b]single-crystal X-ray diffraction; [c]powder X-ray diffraction; [d]pressure interval of the experiment/calculation; [e]volume measurement at ambient conditions using SCXRD; [f]estimated volume at ambient conditions; [g]alternatively K_0 = 125 (3) and K_0' = 3.8 (2); [h]alternatively K_0 = 112 (1) and K_0' = 4.3 (1); [i] density functional theory calculations; [j]Brillouin spectroscopy

The following equations were used for the calculation of V_P and V_S uncertainty:

$$\sigma_{V_S} = \frac{1}{2}\rho^{-1}(G\rho^{-1})^{-1/2}\sigma_G \quad \text{(Eq. S1)}$$

$$\sigma_{V_P} = \left[\rho^{-2}{V_P}^{-2}\left(\frac{4}{9}{\sigma_G}^2 + \frac{1}{4}{\sigma_K}^2\right)\right]^{1/2} \quad \text{(Eq. S2)} \ ,$$

where ρ is density, G is bulk modulus, σ_G is the standard deviation in shear modulus and σ_K is the standard deviation in bulk modulus.

The ratio between phonon creation energies (S(E)) and phonon annihilation energies (S(-E)) is given by the Boltzmann factor as follows:

$$S(E) = e^{\beta E}S(-E) \quad \text{(Eq. S3)} \ ,$$

where $\beta = 1/(k_\beta T)$ is the inverse temperature, and k_β the Boltzmann constant. With these equations, we can estimate the sample temperature using the NIS signal.

The following equations describe the linear relation (see also Figure 6) of depth (d in km) with the averaged elastic wave velocity values (V_S and V_P in km/s) that we obtained from our $FeCO_3$ and $(Mg_{0.74}Fe_{0.26})CO_3$ samples using the NIS method:

<u>High spin – $(Mg_{0.74}Fe_{0.26})CO_3$:</u>

$$V_S = 0.0006 \cdot d + 4.2(2) \text{ and } V_P = 0.002 \cdot d + 7.7(4) \quad \text{(Eq. S4)}$$

<u>Low spin – $(Mg_{0.74}Fe_{0.26})CO_3$:</u>

$$V_S = 0.0003 \cdot d + 5.0(3) \text{ and } V_P = 0.0012 \cdot d + 9.1(7) \quad \text{(Eq. S5)}$$

<u>High spin – $FeCO_3$:</u>

$$V_S = 0.0007 \cdot d + 3.2(1) \text{ and } V_P = 0.002 \cdot d + 6.66(8) \quad \text{(Eq. S6)}$$

<u>Low spin – $FeCO_3$:</u>

$$V_S = 0.0005 \cdot d + 4.09(6) \text{ and } V_P = 0.0013 \cdot d + 8.01(5) \quad \text{(Eq. S7)}$$

Data points from both powder and crystal samples were considered in the averaging procedure. In the case of $FeCO_3$, data points from powder and single-crystal measurements are uniformly scattered (Figure 3c and 6), thus we can assume that the bulk shear wave velocity can be described by equation (S4). In the case of $(Mg_{0.74}Fe_{0.26})CO_3$, nearly all velocities are represented by measurements on a single crystal with unknown orientation (see Cell#2 in Table S1). Given the sensitivity of the NIS method to crystal orientation we recognize that a systematic error may be introduced in our further modeling calculations of other ferromagnesian compositions. However, at ambient conditions the Debye and shear wave velocities between a powder sample and our

single crystal differ only by 5.1% and 5.5%, respectively, which is comparable to the uniform scattering that is observed for the $FeCO_3$ sample. Therefore, all data points of the $(Mg_{0.74}Fe_{0.26})CO_3$ were considered in the averaging procedure. All equations reported above include the data resolution error. In addition, the errors in equations S4 and S5 account for the systematic error that may be introduced when using single crystal data points. Finally, a linear relation and Vegard's law were assumed for the modeling of the $(Mg_{0.85}Fe_{0.15})CO_3$ shear wave velocities that appear in Figure 7.

Table S3. Detailed dataset of heated samples in this study.

Sample	Cell #	Type	PTM[a]	P (GPa)	T (K)	ρ (g/cm^3)	Vd (km/s)
$FeCO_3$	6	pwdr[b]	KCl	22.4(5)	470(50)	4.58(14)	3.98(12)
	6	pwdr	KCl	22.0(5)	296(2)[c]	4.57(14)	3.93(14)
	6	pwdr	KCl	25(2)	1750(100)	4.63(15)	4.40(25)
	8	pwdr	KCl	21(1)	296(2)[c]	4.55(14)	3.85(22)
	8	pwdr	KCl	26(2)	1700(100)	4.64(15)	3.70(15)
	9	pwdr	KCl	58(2)	1100(100)	5.78(6)[d]	3.60(18)
	9	pwdr	KCl	59(2)	1700(100)	5.80(7)[d]	3.60(16)

[a] pressure transmitting medium; [b] powdered sample; [c] measurement on the temperature quenched sample, [d] sample treated as Fe_3O_4 (Bbmm)

Table S4. Calculated minimal amount of carbonate needed to be present at various depths in order to detect seismically a 1 % drop in shear velocities. Note that the composition $(Mg_{0.85}Fe_{0.15})CO_3$ is considered to be the most realistic for the mantle.

Depth (km)	$FeCO_3$	$(Mg_{0.74}Fe_{0.26})CO_3$	$(Mg_{0.85}Fe_{0.15})CO_3$
300	4 wt %	21 wt %	undetectable
600	3 wt %	7 wt %	9 wt %
1000	3 wt %	4 wt %	5 wt %
1450	4 wt %	6 wt %	6 wt %

Supplementary Figures

Figure S1: Variation of Fe–O and (Mg,Fe)-O bond lengths for $FeCO_3$ and $(Mg_{0.74}Fe_{0.26})CO_3$ with increasing pressure, respectively. Error bars are shown, and in some cases, are smaller than the size of the symbols.

Figure S1

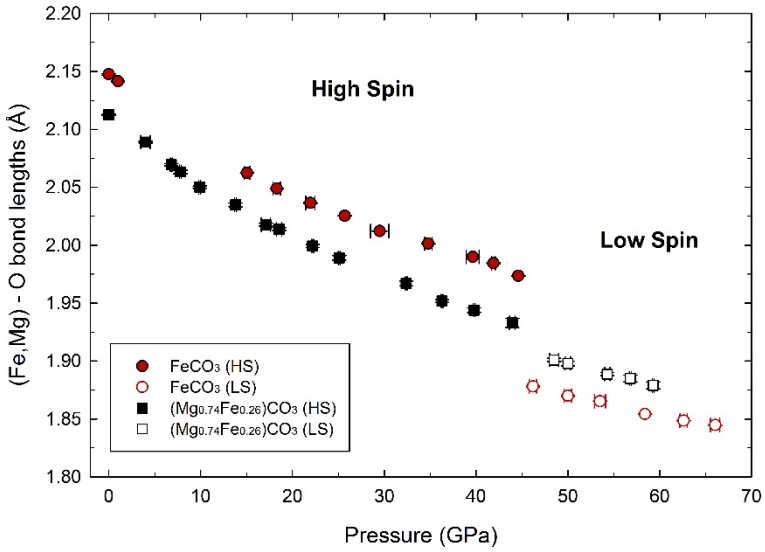

Figure S2: Variation of C–O bond lengths within the CO_3 unit for $FeCO_3$ and $(Mg_{0.74}Fe_{0.26})CO_3$ with increasing pressure.

Figure S2

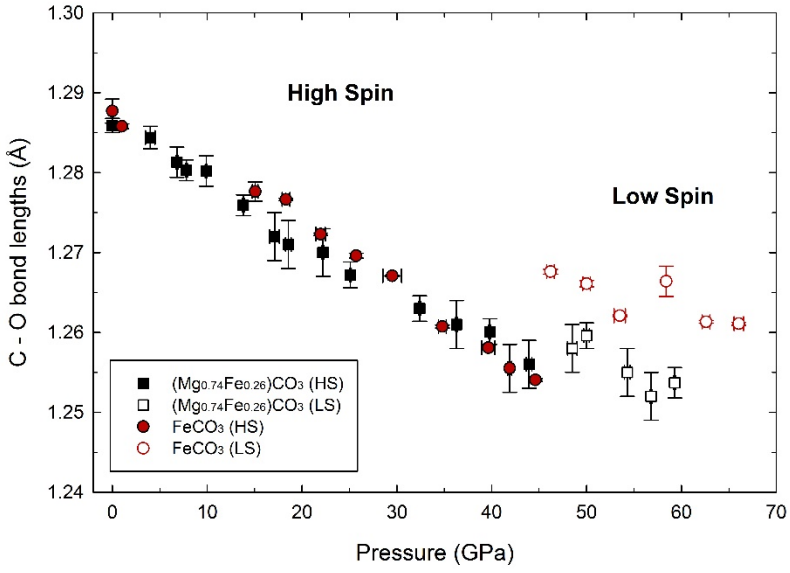

Figure S3: Effect of 20 % increase in bulk modulus on the calculation of V_P. The new values (dashed lines) of this study are compared to the previous study by Stekiel et al. (2017) (bold lines). Although we note that the nature of the samples used in this study and the one of Stekiel et al. (2017) is not the same, the graph illustrates the strong influence of the choice of bulk modulus on V_P.

Figure S3

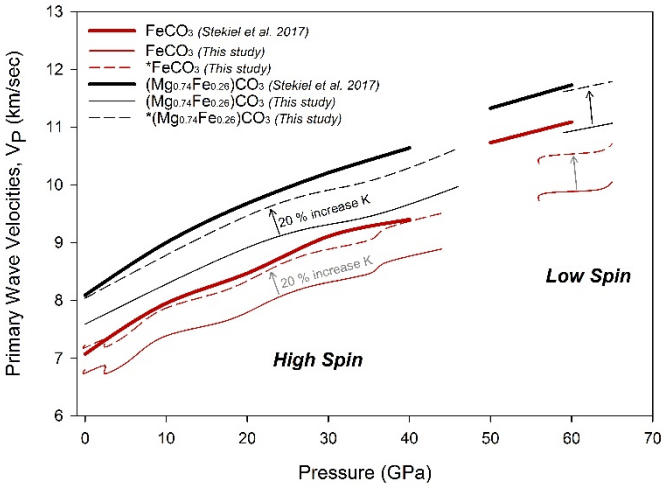

Figure S4: Modeling the effect of mixed Fe spin state compared to Debye velocities of heated $FeCO_3$ at high pressure. Reduced values account for a ~60% drop of primary wave velocities according to Fu et al. (2017) and Equation 2 (main text). The reduced values are not low enough to explain the Debye velocity drop that we observed using NIS. Pressure determination using ruby fluorescence before and after laser heating confirmed that the sample remained under high pressure. The grey dashed line is a guide to the eye showing V_D of $FeCO_3$ at ambient conditions. The heated data (red squares) fall below this line, further suggesting that the two measurements do not correspond to $FeCO_3$ at 1 bar.

Figure S4

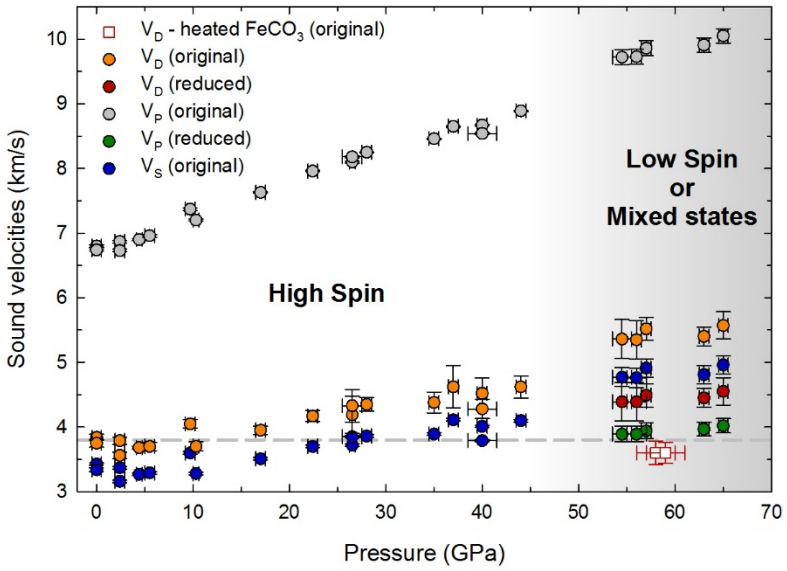

Additional References:

Lin, J-F., Liu, J., Jacobs, C., and Prakapenka, V.B. (2012) Vibrational and elastic properties of ferromagnesite across the electronic spin-pairing transition of iron. American Mineralogist, 97, 583-591.